A Communication Link Analysis Based on Biological Implant Wireless Body Area Networks

Yangzhe Liao, Mark S. Leeson, and Matthew D. Higgins

School of Engineering
University of Warwick, Coventry, CV4 7AL, UK
{yangzhe.liao, mark.leeson, m.higgins}@warwick.ac.uk

Abstract ─ The rapid growth in remote healthcare services and biomedical demands has seen novel developments in wireless body area networks (WBANs). The WBAN can be seen as an integration of intelligent networks, which permits devices and sensors to work together to obtain a series of critical physiological parameters, such as blood flow velocity and heartbeat frequency. Analysis of WBAN radio frequency communication systems is the key factor and the critical research challenge that determines system performance, such as achievable transmission distance, data rate and so forth. The human head is an area of particular potential in WBAN design that is worthy of attracting more attention than its limited literature to date. This paper is primarily focused on the one of the most detailed comprehensive multi-modal imaging-based anatomical human head models. This is a multimodal imaging-based detailed anatomical model, denoted by the acronym MIDA, this features 153 structures at a high resolution of up to 500 μm, including numerous distinct muscles, bones and skull layers in the license-free 2.4 GHz industrial, scientific, and medical (ISM) band. It presents and compares a set of advanced simulation methods and then proposes a path loss simulation flat phantom, semi-empirical path loss models for typical homogeneous tissues and the anatomical human head MIDA model. The bit error rate (BER) performances of the MIDA model fading channel using binary phase shift keying (BPSK) and pulse-amplitude modulation (PAM) are obtained. Furthermore, achievable transmission distances for several data rates for predetermined acceptable BERs are accomplished. The results show that PAM promises longer transmission distances than BPSK when using both high and low data rates. The proposed communication systems can be applied to optimize implantation communication system scenarios and biotelemetry applications.

Index Terms ─ MIDA human head model, path loss, system margin, WBANs.

I. INTRODUCTION

Wireless body area networks (WBANs) are becoming increasingly significant for numerous applications in e-health and biosensor technology for a number of reasons, including low power consumption, simple structure requirements and potentially fast transmission data rates [1-3]. A typical WBAN can be regarded as a healthcare network system, which consists of sensors and other devices on, near or inside the human body as shown in Fig. 1. Recently, implant WBANs for biomedical applications have brought about a revolutionary change due to the development of antenna technologies and wireless communication systems [4]. However, surprisingly little work has been published to date on the proposed use of WBANs for the human cephalic section, which is the most significant and urgent area that can cooperate with future telemedicine technology and electronic medical services [4, 5].

An important feature in the development of WBANs is the characterization of the physical layer [4-7]. The majority of the literature has been concerned with on-body propagation while fewer studies have been focused on the modeling of intra-body propagation subjects [8-10]. Since the human body area is a natural lossy environment, signals propagating from the transmitter are attenuated considerably before reaching the receiver; hence an essential step in the understanding of implant WBANs is to comprehend the propagation loss process [11-15]. A path loss (PL) model is an advantageous approach to help with the design of wireless communication systems between nodes located within the human body [13-18]. In [16], the performance of PL in muscle and fat tissues individually is obtained using insulated dipole antennas at 2.45 GHz through a Method of Moments program, FEKO from EMSS in South Africa. In [17], PL results have been obtained for an in-body propagation model in saline water with a Hertzian dipole. A multi-implant setup at 2.4 GHz has been investigated in [18] using insulated dipole antennas for specific locations including the liver, heart, spleen and

Submitted On: September 18, 2015
Accepted On: March 18, 2016

kidneys.

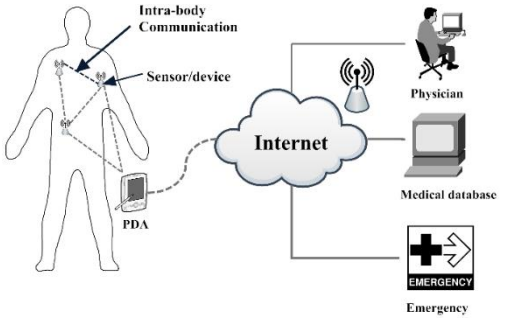

Fig. 1. Typical architecture of an implant WBAN system.

Due to the difficulty of specific absorption rate (SAR) measurements in an actual human head for electromagnetic (EM) radio-frequency exposure, the second challenge lies in the examination of human tissue safety [19, 20]. This involves evaluating health risks related to exposure to electromagnetic (EM) fields and making sure that these satisfy the international SAR compliance regulations, for example those of the Institute of Electrical and Electronics Engineers (IEEE) [21] and the International Commission on Non-Ionizing Radiation Protection (ICNIRP) [22].

Implant WBAN analysis includes propagation loss, energy consumption, transmission rate, and quality transmission distance issues [1-5]. Shadow fading characterizes the variations in the implant WBAN channel power loss caused by obstacles in the propagation path [23]. Also, essential requirements within an implant WBAN channel model are the capability to support long transmission distances and high transmission data rates that can effectively connect and work with future medical servers [24, 25].

The work described in the present paper is intended to provide valuable insight into implantable communication systems research. The rest of the paper is organized as follows. Frequency selection and EM simulation methods are discussed and selected in Section II [23, 24, 26-28]. In Section III, a PL simulation flat phantom is proposed and semi-empirical PL models for typical homogeneous tissues as well as the MIDA cephalic model are given. A flat phantom is utilized to obtain the properties of various typical homogeneous tissues, in which the signal propagation attenuation is determined using a transmitting dipole antenna (Tx) and receiving dipole antenna (Rx). Then semi-empirical PL models for several typical human tissues are proposed as well as the MIDA human head model [29]. This is followed by calculation of the maximum 10-g SAR distribution [21, 22]. In Section IV, several performance indicators are determined using binary phase shift keying (BPSK) and pulse-amplitude modulation (PAM), and the MIDA cephalic model fading channel. The indicators are the bit error rate (BER) performance, the minimal signal-to-noise ratio (SNR) requirement, the system margins and the achievable transmission distances for several data rates at a given BER. Finally, Section V presents conclusions and suggestions for further work.

II. RELATED WORK

Selecting the frequency for the WBAN system can profoundly influence tissue dielectric characterization as well as implanted antenna size [23-28]. WBAN channels are primarily proposed in the medical implant communication service (MICS), industrial, scientific, and medical (ISM) and the ultra wideband (UWB) frequency bands or in multi-bands [5]. The MICS frequency band allows the transmitted signal to suffer lower attenuation when propagating along an implanted communication path than the UWB and ISM bands, and was thus accepted for the IEEE 802.15.6 standard [29]. However, the MICS band is less likely to satisfy future high data transmission demands; it results in antennas that are too large and complex to employ in realistic situations [6, 29-31]. The UWB frequency band is a promising candidate due to its simple structure, multi-path fading, and high data speed. Nevertheless, the weaknesses of UWB are that it only offers short-range of coverage and it experiences higher energy attenuation [2, 6, 26, 32]. In this paper, the 2.4 GHz band is selected because it can support higher data rate applications and is accepted worldwide [6]. The results indicate that higher transmitted power within safety guidelines can be obtained. It is also much more likely to be embedded within the human body due to its small antenna size.

Numerous advanced electromagnetic simulation technologies have been applied in WBANs [13, 15, 16, 33-35]. In [33], it was pointed out that the method of moments (MoM) is the most effective technology for planar antenna structures (for example, PCB layers). The finite element method (FEM) is a useful scheme for helical antennas along with some simple 3D constructions [34]. Unlike the MoM and FEM algorithms, the finite difference time domain (FDTD) approach [35] is very efficient for solving complex problems, such as the characterization of antenna performance when embedded inside multi-layer surroundings. In addition, FDTD 3D model meshes are built from Yee Cells so as to deliver high processing capabilities and reduced memory resources for large 3D structures [35]. It is important to note that, unlike much other work, which uses conductivity and relative permittivity to simulate tissues in the High Frequency Structure Simulator (HFSS) and other commercial software [4-5, 12, 16, 41-43], here we employ the CST Studio Suite® 2015 (Computer Simulation Technology, Darmstadt, Germany) [36] which takes the loss tangent parameter into account. Moreover, at the same time relatively permittivity is automatically

considered in the simulation process, thus allowing the simulation results to be more accurate [3, 36-39].

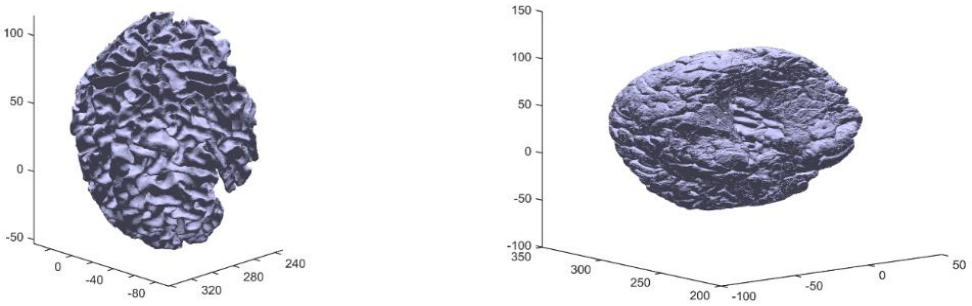

Fig. 2. MIDA 3D model structures of brain white matter (left) and brain gray matter (right). (Units in millimeters).

Given the difficulty of experimental investigation of signal power loss on a real human body, the CST program has been investigated for solving electromagnetic issues in this paper. The multimodal imaging-based detailed anatomical or MIDA model [29] was obtained by scanning a healthy 29-year old female volunteer head and neck down to the level of the fifth cervical vertebra at the Institute for Biomedical Engineering Laboratory (ETH, Zurich, Switzerland). It is a detailed anatomical computer model, including 153 kinds of different organs and tissues, with a highest resolution of 0.5 mm; it is thus more advanced and accurate than the Virtual Family models [38-40]. The advances of the MIDA model are not limited to computational modeling research, but also can be applied to computational simulations to investigate the safety and efficacy of medical devices located in, on or around the head [29]. Figure 2 shows the brain white matter and brain gray matter of the MIDA model.

III. PL MODELING AND HUMAN SAFETY ANALYSIS

A. Simulation setup

For traditional wireless communication, radio propagation refers to the process of radio waves suffering from reflection, diffraction and scattering when they propagate from the Tx to the Rx [1-4]. However, the scenario of in-body communication channel is more complicated and less predictable as the intensity varies with the lossy environment at diverse locations. As we are mainly aiming to design communication links within a human head model, the antenna design issue is not the central focus of this paper. To the best of our knowledge, the majority of the proposed antennas for in-body communication systems use a homogenous tissue (single layer structure), and are unable to work accurately when embedded in the brain, which is a multi-layer structure [16, 17, 42]. Kurup et al. proposed a novel insulated dipole antenna rather than bare dipoles for WBANs at 2.45 GHz [16]. The method improves the leakage of conducting charge as well as reducing sensitivity of the current distribution within the ambient medium. However, the dielectric parameters of the insulator material polytetrafluoroethylene are similar to those of human muscle tissue and can thus affect the simulation results. In this paper, two identical dipoles are selected because dipole antennas are simple and well-understood in free space communications. Additionally, the dimensions of such antennas are appropriate for them to be implanted in the body [16, 41]. The two arms of the dipole antenna (shown in Fig. 3) are both made of perfect electric conducting (PEC) material with a diameter λ_1 = 1 mm. The resonance occurs when the antenna is equal to a half wavelength in a transmission medium, and λ_2 = 6.25 cm for 2.4 GHz. The simulations use a voltage source, and the dimensions and simulation methods are the same for all the cases examined. The proposed flat phantom is beneficial to understand and compare the PL performance between several typical human head tissues Also, antenna design mechanisms can be applied to the MIDA model. The dielectric parameters are frequency dependent and can be obtained from thorough survey published by Andreuccetti et al. [44]. This was compiled using both data from a range of published papers and comprehensive measurements by the authors using several experimental techniques. Figure 4 demonstrates that tissue conductivity is monotonically increasing while the loss tangent goes through a minimum close to 2.5 GHz. The dielectric parameters of several typical human tissues at 2.4 GHz, such as conductivity σ, loss tangent $\tan\delta$ and relative permittivity ϵ_r, are summarized in Table 1 [44].

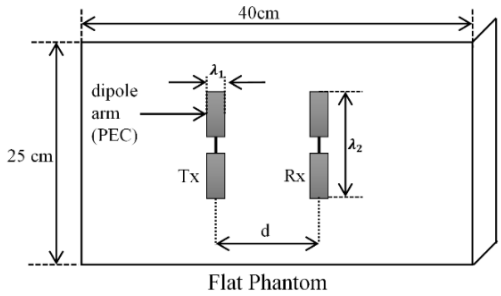

Fig. 3. Simulation platform design.

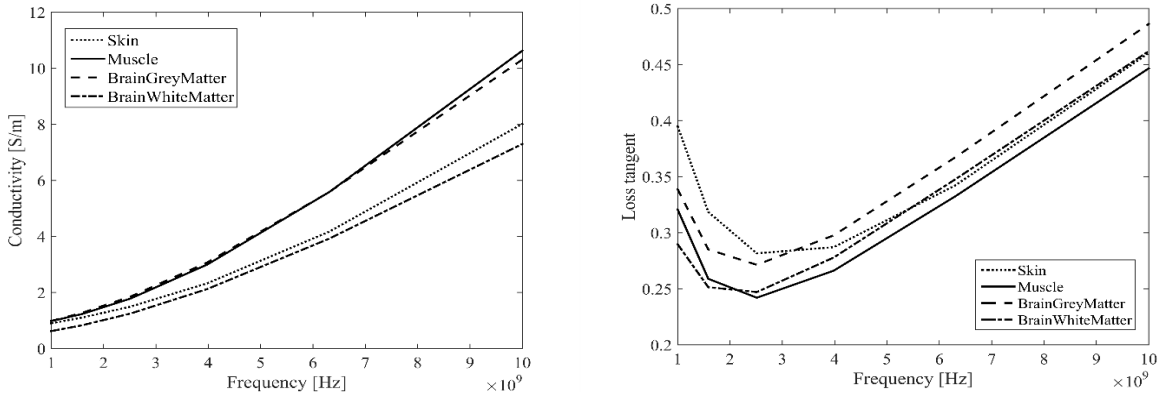

Fig. 4. (left) Conductivity of skin, muscle, brain gray matter and brain white matter from 1-10 GHz. (right) Loss tangent of skin, muscle, brain gray matter and brain white matter from 1-10 GHz.

B. PL analysis

We first investigate wave propagation at 2.4 GHz in human homogeneous tissues, using simulations for the proposed implantable antennas. The dielectric parameters used are those summarized in Table 1. The simulations in this paper are all performed using the 3D CST FDTD electromagnetic solver introduced above. The maximum grid step in the homogeneous tissues and heterogeneous MIDA human head model is 1 mm. The simulations are carried out using the implantable antennas up to 5 cm apart for homogeneous tissues.

Table 1: Dielectric properties of human body typical tissues at 2.4 GHz [44]

Tissue	σ	ϵ_r	$tan\,\delta$
Dry skin	1.441	38.063	0.2385
Muscle	1.705	52.791	0.2419
Brain gray matter	1.773	48.994	0.2710
Brain white matter	1.190	36.226	0.2460

Figure 5 shows that the direction of the Tx and Rx dipole antennas are both set to be aligned in the MIDA model. The Tx transmitting dipole is fixed in the skin tissue while the Rx receiving dipole horizontally moves from the reference location (d = 0.5 cm) up to a distance of 7 cm (from the skin area to the deep head area). The scenario of the simulated PL of MIDA (heterogeneous model) is more complex than homogeneous tissues because energy attenuation becomes considerable and antenna coupling occurs when penetrating other tissues alone. The PL is derived as a function of the distance between Tx and Rx when the antennas are aligned for homogeneous tissues and a heterogeneous human head model. A semi-empirical in-body distance-based PL model in dB based on the Friis formula [16, 24, 44] is proposed:

$$PL_{dB}(d) = \alpha + 10n\log_{10}(d) + S, \qquad (1)$$

where α denotes the PL value at d_{ref} (set as 0.05 cm). The variable d is the separation distance between the Tx and Rx antennas. The PL model allows the receiving antenna at the same distance d to have a different PL, which varies with a normally distributed, zero mean random shadowing effect $S \sim \mathcal{N}(0,\sigma^2)$. The value of the variance for the MIDA model may be taken from the standard deviations given in Table 2. This contribution thus explicitly includes the stochastic effect of shadow fading that is imposed on the deterministic contribution to the PL. The parameter n represents the standard PL exponent; this varies with the transmission medium, with a value of two corresponding to free space and higher values including situations with more obstructions. To assess the accuracy of the parameter estimates, a least square fit method and MATLAB curve fitting toolbox were applied to determine PL [42] with the detailed information summarized in the last row of Table 2. The coefficients of determination values R^2, representing the fitting degree between PL and the antenna separation distances, are higher than those mentioned in [16, 44] indicating a better fit.

Figure 6 shows PL results illustrating that the highest PL value is achieved by muscle, followed by brain gray matter, brain white matter and then skin. The simulation starts at d = 5 mm from the transmitting antenna and ranges up to a distance of 5 cm for homogeneous tissues in order to limit antenna coupling effects [42]. The results are similar to those seen previously in the literature [5, 6], although previous work used insulated or helical antennas. As expected, the PL increases when the separation distance between Tx and Rx increases. Figure 7 shows the PL as a function of the distance of the proposed heterogeneous MIDA model. The PL is derived as a function of the distance between Tx and Rx when the antennas are aligned for homogeneous tissues and a heterogeneous human head model.

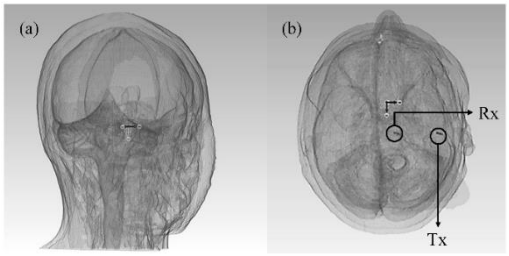

Fig. 5. MIDA model and dipole antennas. (a) side view, and (b) front view.

Table 2: Parameters for PL models for homogeneous tissues and the MIDA model

Tissue	α	n	σ	R^2
Dry skin	30.17	1.608	1.534	0.9941
Muscle	37.08	1.964	3.623	0.9911
Brain gray matter	37.97	1.631	0.658	0.9972
Brain white matter	36.97	1.644	1.101	0.9954
MIDA model	43.95	2.552	1.079	0.9728

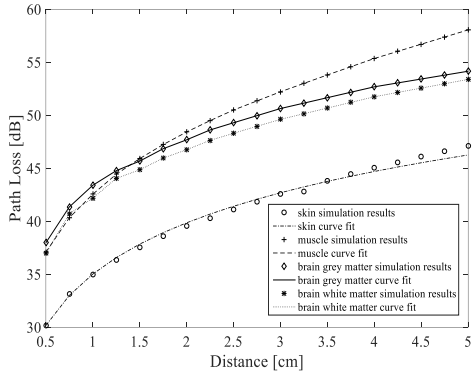

Fig. 6. PL versus separation distance between antennas for homogeneous tissues.

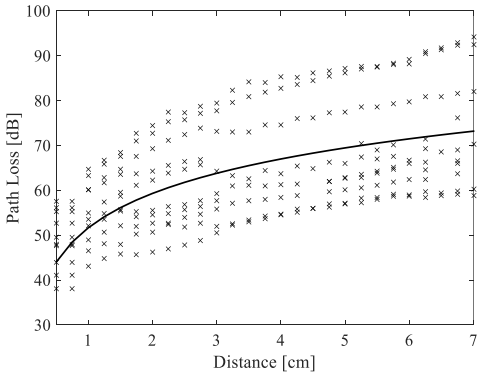

Fig. 7. PL versus distance between antennas for heterogeneous human body model.

C. Human tissues safety

As the human head is an extremely sensitive environment with tissues absorbing electromagnetic power from the antenna [19], safety is paramount. Therefore, we undertook numerical SAR calculations for comparison to latest regulatory authority provisions. For example, the IEEE standard regulates the SAR averaged over 10g of tissue to no more than 1.6 W per kg in the shape of a cube [21]. The ICNIRP regulations state that the limit of the average SAR of 10g contiguous tissue should be less than 2 W per kg [22].

It can be seen from Fig. 8 that the maximum SAR 10g W per kg changes with the distance. SAR values have been calculated by moving the Rx antenna position in the human head. The maximum value is 0.14 W per kg at the nearest point of skin tissue and the lowest SAR value is 0.045 W per kg at a distance of approximately 2 cm from the reference point.

Figure 9 presents the relationship between absorbed that the maximum power is 3.8 mW at the reference point while the minimum value of 1.9 mW occurs between 2 and 2.5 cm from the reference point. These SAR and absorbed power results reveal that the antenna design and simulation methods are suitable and meet the safety requirements of the ICNIRP and IEEE standards [21, 22].

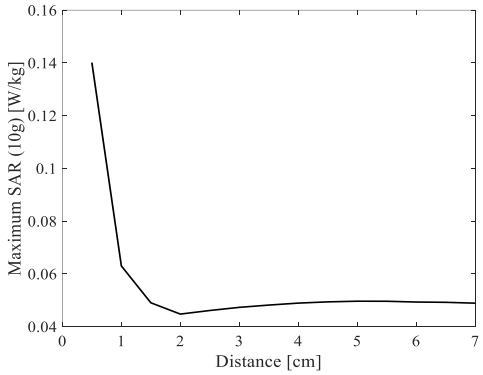

Fig. 8. Influence of the distance on the maximum SAR over 10g.

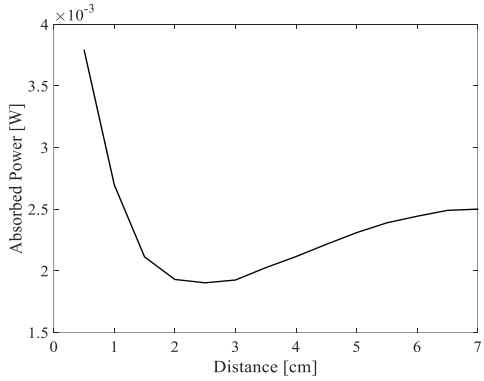

Fig 9. The absorbed power versus antennas separation distance.

IV. SHADOW FADING CHANNEL MODELING AND SYSTEM MARGIN

It is difficult to analytically derive the probability density function of the combined SNR at the receiver output. Therefore, we employ an approximation based on curve fitting and the results are shown by the solid line on Fig. 7 based on the least square error [44]. As can be seen from that figure, there is a large fluctuation in the simulated path loss values around the fitted mean path loss. The fluctuation of the simulated path loss is mainly due to the shadowing effect of the different brain tissues. The shadowing is induced by the diffraction in the shadowed regions of the body [45-46].

Since body motions are not considered in this paper, a static human body model is assumed. Shadowing can be regarded as directly resulting in the variations of the received signal at the receiver front-end. The amplitude variation caused by shadowing is often defined as the difference between calculated path loss values and the mean path loss. The mean PL is denoted by PL_{dB}^{ave}, which based on the empirical power decay law is a potential PL model for fitting to the calculated results [6, 16, 24, 44]:

$$PL_{dB}^{ave}(d) = \alpha + 10n \log_{10}\left(\frac{d}{d_{ref}}\right), d \geq d_{ref}, \quad (2)$$

where α is the PL at the reference point (0.5 cm) andequals 43.95 dB; the PL exponent *n* is here 2.552.

The shadow fading effect *S* can be derived from Equations (1) and (2):

$$S_{dB} = PL_{dB}(d) - PL_{dB}^{ave}(d). \quad (3)$$

The in-body communication channel might have a different PL since the surrounding environments may vary with the location of the receiver in practice. However, the majority of published PL models do not take this particular situation into account [1-3, 16]. A log-normal shadowing model is appropriate when dealing with a more realistic situation and the shadow fading *S* follows a lognormal distribution, which can be expressed as [13, 44, 46-47]:

$$p(S) = \frac{1}{\sqrt{2\pi}\sigma S} exp\left[-\frac{(\log_{10}(S)-\mu)^2}{2\sigma^2}\right], \quad (4)$$

where *S* has mean μ and standard deviation σ. Here, we take $\mu = 0$ and $\sigma = 1.079$. The average BER of the human head shadow fading channel can be expressed as [13, 19]:

$$P_b(\bar{\gamma}) = \int_0^\infty P_0(\gamma)P(\gamma)d\gamma, \quad (5)$$

where $\bar{\gamma}$ is the mean signal-to-noise ratio, $P_0(\gamma)$ denotes the BER performance of the additive white Gaussian noise (AWGN) channel, and $P(\gamma)$ is the probability density function of γ which follows a lognormal distribution with the same standard deviation as the BER performance for this shadow fading channel using BPSK and binary orthogonal PAM using the MIDA model is shown in Fig. 10.

In common with previous work on in-body communication systems [16, 18], to provide acceptable quality for communication, the predetermined threshold BER is set as 10^{-3} for both BPSK and binary orthogonal PAM optimum receivers [15-17, 44]. With this value of BER, it can be seen from Fig. 10 that the minimum required SNR_{min} of binary orthogonal PAM is around 10.5 dB, while for BPSK it is nearly 17 dB.

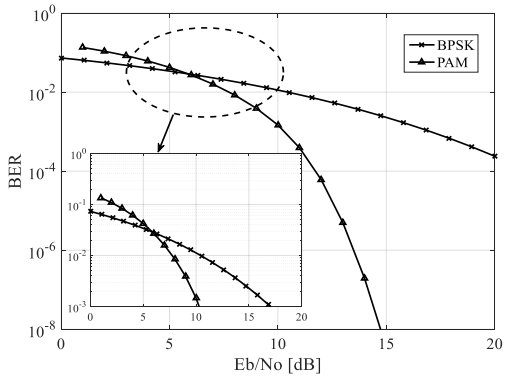

Fig. 10. SNR versus BER under the MIDA human head model fading channel under the BPSK and binary orthogonal PAM modulation schedules.

It is then necessary to take into account the wireless communication systems link budget. According to the existing literature [3, 4, 9, 45], AWGN noise at the receiver side is the only noise source which needs to be considered, basically representing thermal noise. The one-sided power spectral density of the noise in Watts per Hertz (dimensionally equivalent to Joules) is given by:

$$N_0 = k[T_a + (N_F - 1)T_0], \quad (6)$$

where T_a and T_b are the noise temperature of the receiving dipole antenna and of the environment, respectively, k is the Boltzmann constant and N_F is the noise factor at the receiver side. This is defined via the noise figure in dB by:

$$N_{F,dB} = 10\log_{10}(N_F), \quad (7)$$

where the noise factor of an intra-body device is related to its noise temperature T_e by:

$$N_F = 1 + \frac{T_e}{T_0}. \quad (8)$$

We assume the temperatures of the Tx and Rx antennas are the same since they are both located in the human head. Noise temperature (thermal noise), which depends on the temperature of the intra-body device, thus can be seen as the same as T_0:

$$T_a = T_0, \quad (9)$$

$$T_0 = T_e. \quad (10)$$

The mean temperature of the human head over baseline is 36.56 °C (equal to 309K), with a standard deviation of 0.36 °C and a range from 36.16 °C to 37.02 °C [48]. Equation (6) can be rewritten in dB scale as:

$$N_{0,dB} = 10\log_{10}(kT_0) + N_{F,dB}. \quad (11)$$

The SNR in dB thus can be expressed as:

$$SNR_{dB} = P_{r,dBW} - 10\log_{10}(R_b) - N_{0,dB}, \quad (12)$$

where $P_{r,dBW}$ is the received power and R_b is the communication transmission data rate.

A system margin M_s [49] is introduced to evaluate the quality of the communication system channel; it is also an effective way of evaluating system performance when a predetermined BER (10^{-3}) is selected. This system margin M_s can be taken as:

$$M_s = SNR_{dB} - SNR_{min} \geq 0, \quad (13)$$

where SNR_{min} is the minimal SNR value that promises a reliable communication transmission in the predetermined BER situation.

Figure 11 illustrates the achievable quality transmission distance at a number of data rates of 1 Mbps, 10 Mbps and 20 Mbps employing BPSK and binary orthogonal PAM modulation. It can be seen that the implanted communication link can achieve higher data rates at shorter distances. For BPSK, 20 Mbps can be reliably transmitted at a distance of around 4.5 meters and 10 Mbps can be transmitted at approximately 5.5 meters; using 1 Mbps extends the distance to more than 10 meters. The performance of PAM at those three transmission data rates can reach longer distances than BPSK, and 20 Mbps high speed data transmission rate can be conveyed for up to 8 meters.

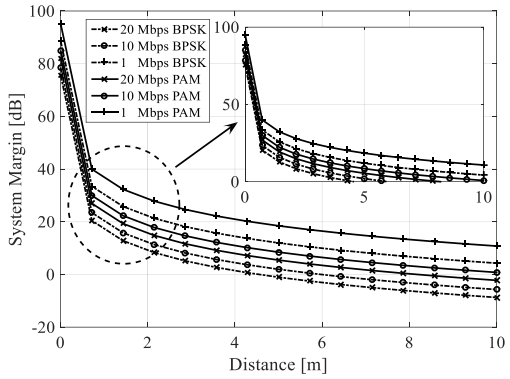

Fig. 11. System margin versus distance at different data rates.

V. CONCLUSION

Implanted WBAN technology is one of the most promising emerging applications in future healthcare services that allows a wide range of applications to function inside the human body. However, there is a limited amount of literature focused on the communication systems for within the human brain. In this paper, a communication link for the human cephalic area has been proposed for implant WBAN communications and analysed using the FDTD method. The BER performances have been obtained using binary orthogonal PAM and BPSK modulation, and the minimal required SNR values for predetermined BER conditions of 10^{-3} are 10.5 dB and 17 dB, respectively. The achievable distances to deliver the target BER are greater with PAM than BPSK for both a higher data rate of 20 Mbps and a relatively lower data rate of 1 Mbps. The results show that a data rate of 20 Mbps to 8 meters can be covered using binary orthogonal PAM but only up to 4.5 meters when employing BPSK. These results point towards future work in the area of in-body cephalic area circuit design and experimental validation.

REFERENCES

[1] T. Tuovinen, et al., "Effect of the antenna-human body distance on the antenna matching in UWB WBAN applications," in *7th Medical Information and Communication Technology (ISMICT) International Symposium*, Tokyo, Japan, pp. 193-197, 2013.

[2] M. Seyedi, B. Kibret, D. T. Lai, and M. Faulkner, "A survey on intrabody communications for body area network applications," *IEEE Transactions on Biomedical Engineering*, vol. 60, no. 8, pp. 2067-2079, 2013.

[3] S. Ullah, et al., "A comprehensive survey of wireless body area networks," *Journal of Medical Systems*, vol. 36, pp. 1065-1094, 2012.

[4] S. Woo, J. Baek, D. Kang, J. Tak, and J. Choi, "A compact UWB MIMO antenna with enhanced isolation for WBAN applications," in *2014 International Symposium on Antennas and Propagation (ISAP)*, Kaohsiung, Taiwan, pp. 413-414, 2014.

[5] K. Y. Yazdandoost, "UWB loop antenna for in-body wireless body area network," in *7th European Conference on Antennas and Propagation (EuCAP)*, Gothenburg, Sweden, pp. 1138-1141, 2013.

[6] B. Choi, et al., "Narrowband physical layer design for WBAN system," in *2010 First International Conference on Pervasive Computing Signal Processing and Applications (PCSPA)*, Harbin, China, pp. 154-157, 2010.

[7] A. Pantelopoulos and N. G. Bourbakis, "A survey on wearable sensor-based systems for health monitoring and prognosis," *IEEE Transactions on Systems, Man, and Cybernetics, Part C: Applications and Reviews*, vol. 40, no. 1, pp. 1-12, 2010.

[8] C. Lee, et al., "Physical layer designs for WBAN systems in IEEE 802.15.6 proposals," in *9th International Symposium on Communications and Information Technology*, Incheon, Korea, pp. 841-844, 2009.

[9] H. Wang, X. Tang, C. Choy, and G. Sobelman, "Cascaded network body channel model for intra-body communication," *IEEE Journal of Biomedical and Health Informatics*, Available online, Doi:10.1109/JBHI.2015.2448111, 2015.

[10] X. M. Chen, S. H. Pun, Y. M. Gao, P. U. Mak, M. I. Vai, and M. Du, "Study on transfer function of intra-body communication based on quasi-static electric field modeling," in *IEEE-EMBS International Conference on Biomedical and Health Informatics (BHI)*, Hong Kong, China, pp. 388-391, 2012.

[11] K. Takizawa et al., "Channel models for wireless body area networks," in *30th Annual International Conference of the IEEE Engineering in Medicine and Biology Society*, Vancouver, Canada, pp. 1549-1552, 2008.

[12] K. L. L. Roman, G. Vermeeren, A. Thielens, W. Joseph, and L. Martens, "Characterization of path loss and absorption for a wireless radio frequency link between an in-body endoscopy capsule and a receiver outside the body," *EURASIP Journal on Wireless Communications and Networking*, vol. 2014, pp. 1-10, 2014.

[13] D. Kurup, et al., "Simulation of path loss between biocompatible antennas embedded in homogeneous human tissues and comparison of their specific absorption rate," in *IEEE Antennas and Propagation Society International Symposium (APSURSI)*, Toronto, Canada, pp. 1-4, 2010.

[14] M. Pourhomayoun, Z. Jin, and M. L. Fowler, "Accurate localization of in-body medical implants based on spatial sparsity," *IEEE Transactions on Biomedical Engineering*, vol. 61, no. 2, pp. 590-597, 2014.

[15] B. Blaszczyszyn, M. K. Karray, and H. P. Keeler, "Wireless networks appear Poissonian due to strong shadowing," *IEEE Transactions on Wireless Communications*, vol. 14, no. 8, pp. 4379-4390, 2015.

[16] D. Kurup, W. Joseph, G. Vermeeren, and L. Martens, "In-body path loss model for homogeneous human tissues," *IEEE Transactions on Electromagnetic Compatibility*, vol. 54, no. 3, pp. 556-564, 2012.

[17] S. K. S. Gupta, Y. Prakash, E. Elsharawy, and L. Schwiebert, "Towards a propagation model for wireless biomedical applications," *Proc. IEEE Int. Conf. Commun*., Anchorage, AK, pp. 1993-1997, 2003.

[18] D. Kurup, W. Joseph, G. Vermeeren, and L. Martens, "Specific absorption rate and path loss in specific body location in heterogeneous human model," *IET Microwaves, Antennas & Propagation*, vol. 7, no. 1, pp. 35-43, 2013.

[19] S. Wolf, D. Diehl, M. Gebhardt, J. Mallow, and O. Speck, "SAR simulations for high-field MRI: How much detail, effort, and accuracy is needed?," *Magnetic Resonance in Medicine*, vol. 69, no. 4, pp. 1157-1168, 2013.

[20] H. Homann, et al., "Local SAR management by RF shimming: A simulation study with multiple human body models," *Magnetic Resonance Materials in Physics, Biology and Medicine*, vol. 25, no. 3, pp. 193-204, 2012.

[21] "IEEE recommended practice for radio frequency safety programs, 3 kHz to 300 GHz," *IEEE Std. C95.7-2005*, pp. 1-52, 2006.

[22] International Commission on Non-ionizing Radiation Protection, "Guidelines for limiting exposure to time-varying electric and magnetic fields (1 Hz to 100 kHz)," *Health Physics*, vol. 99, no. 6, pp. 818-836, 2010.

[23] M. S. Uddin, N. B. Z. Ali, and N. H. Hamid, "Wave propagation and energy model for dynamic wireless body area networks," in *International Conference on Electrical, Control and Computer Engineering (INECCE)*, Kuantan, Malaysia, pp. 160-165, 2011.

[24] A. Kiourti and K. S. Nikita, "A review of implantable patch antennas for biomedical telemetry: challenges and solutions [Wireless Corner]," *IEEE Antennas and Propagation Magazine*, vol. 54, no. 3, pp. 210-228, 2012.

[25] T. Dissanayake, K. P. Esselle, and M. R. Yuce, "Dielectric loaded impedance matching for wideband implanted antennas," *IEEE Transactions on Microwave Theory and Techniques*, vol. 57, no. 10, pp. 2480-2487, 2009.

[26] K. Y. Yazdandoost and R. Kohno, "UWB antenna for wireless body area network," in *Asia-Pacific Microwave Conference*, Yokohama, Japan, pp. 1647-1652, 2006.

[27] A. Alomainy and H. Yang, "Modeling and characterization of biotelemetric radio channel from ingested implants considering organ contents," *IEEE Transactions on Antennas and Propagation*, vol. 57, no. 4, pp. 999-1005, 2009.

[28] M. L. Scarpello, et al., "Design of an implantable slot dipole conformal flexible antenna for biomedical applications," *IEEE Transactions on Antennas and Propagation*, vol. 59, no. 10, pp. 3556-3564, 2011.

[29] M. I. Iacono, et al., "MIDA: A multimodal imaging-based detailed anatomical model of the human head and neck," *PloS One*, vol. 10, no. 4, 2015.

[30] N. Cho, T. Roh, J. Bae, and H. J. Yoo, "A planar MICS band antenna combined with a body channel communication electrode for body sensor network," *IEEE Transactions on Microwave Theory and Techniques*, vol. 57, no. 10, pp. 2515-2522, 2009.

[31] J. Abadia, et al., "3D-spiral small antenna design and realization for biomedical telemetry in the

MICS band," *Radio Engineering*, vol. 18, no. 4, pp. 359-367, 2009.

[32] D. Porcino and W. Hirt, "Ultra-wideband radio technology: Potential and challenges ahead," *IEEE Communications Magazine*, vol. 41, no. 7, pp. 66-74, 2003.

[33] V. Vahrenholt, et al., "Fast EMC analysis of systems consisting of PCBs and metallic antenna structures by a hybridization of PEEC and MoM," *IEEE Transactions on Electromagnetic Compatibility*, vol. 52, no. 4, pp. 962-973, 2010.

[34] N. Neveu, et al., "Miniature hexaferrite axial-mode Helical antenna for unmanned aerial vehicle applications," *IEEE Transactions on Magnetics*, vol. 49, no. 7, pp. 4265-4268, 2013.

[35] F. Demuynck and M. Petersen, "Choosing the right EM simulation technology for antenna design and analysis," in *6th European Conference on Antennas and Propagation (EUCAP)*, Prague, Czech, pp. 1296-1300, 2012.

[36] https://www.cst.com/products/cstmws

[37] K. Kyung Sup, S. Ullah, and N. Ullah, "An overview of IEEE 802.15.6 standard," in *3rd International Symposium on, Applied Sciences in Biomedical and Communication Technologies (ISABEL)*, pp. 1-6, 2010.

[38] M. Iacono, et al., "A computational model for bipolar deep brain stimulation of the sub thalamic nucleus," in *36th Annual International Conference of the IEEE Engineering in Medicine and Biology Society*, Chicago, IL, pp. 6258-6261, 2014.

[39] E. Neufeld, et al., "Simulation platform for coupled modeling of EM-induced neuronal dynamics and functionalized anatomical models," in *7th International IEEE/EMBS Conference on Neural Engineering*, Montpellier, France, pp. 517-520, 2015.

[40] M. C. Gosselin, et al., "Development of a new generation of high-resolution anatomical models for medical device evaluation: The virtual population 3.0," *Physics in Medicine and Biology*, vol. 59, no. 18, pp. 5287, 2014.

[41] H. Y. Lin, M. Takahashi, K. Saito, and K. Ito, "Performance of implantable folded dipole antenna for in-body wireless communication," *IEEE Transactions on Antennas and Propagation*, vol. 61, no. 3, pp. 1363-1370, 2013.

[42] D. Kurup, W. Joseph, G. Vermeeren, and L. Martens, "Path loss model for in-body communication in homogeneous human muscle tissue," *Electronics Letters*, vol. 45, no. 9, pp. 453-454, 2009.

[43] G. Noetscher, Y. Xu, and S. Makarov, "Body area antenna link modeling using MATLAB engine," in *35th Antenna Applications Symposium*, Monticello, IL, pp. 20-22. 2011.

[44] D. Andreuccetti, R. Fossi, and C. Petrucci, "An internet resource for the calculation of the dielectric properties of body tissues in the frequency range 10 Hz-100 GHz," Online: http://niremf.ifac.cnr.it/tissprop/

[45] R. Chavez-Santiago, K. Sayrafian-Pour, A. Khaleghi, K. Takizawa, J. Wang, I. Balasingham, and H. B. Li, "Propagation models for IEEE 802.15.6 standardization of implant communication in body area networks," *IEEE Communications Magazine*, vol. 51, no. 8, pp. 80-87, 2013.

[46] G. D. Ntouni, A. S. Lioumpas, and K. S. Nikita, "Reliable and energy-efficient communications for wireless biomedical implant systems," *IEEE Journal of Biomedical and Health Informatics*, vol. 18, no. 6, pp. 1848-1856, 2014.

[47] M. Cheffena, "Performance evaluation of wireless body sensors in the presence of slow and fast fading effects," *IEEE Sensors Journal*, vol. 15, no. 10, pp. 5518-5526, 2015.

[48] B. Harris, P. Andrews, I. Marshall, T. Robinson, and G. Murray, "Forced convective head cooling device reduces human cross-sectional brain temperature measured by magnetic resonance: A non-randomized healthy volunteer pilot study," *British Journal of Anesthesia*, vol. 100, no. 3, pp. 365-372, 2008.

[49] D. B. Smith, D. Miniutti, L. W. Hanlen, D. Rodda, and B. Gilbert, "Dynamic narrowband body area communications: Link-margin based performance analysis and second-order temporal statistics," in *IEEE Wireless Communications and Networking Conference*, Sydney, Australia, pp. 1-6, 2010.

Yangzhe Liao received his B.S. degree in Measurement and Control Technology from the Northeastern University, China in 2013 where he was also an exchange student in the Electrical and Computer Engineering Department of the University of Illinois at Chicago during his final year. Currently he is a Ph.D. student in the School of Engineering, University of Warwick, UK. His research interests include Wireless body area networks, Mathematical modeling, Error correction and detection codes and communication systems, Multi-input Multi-output systems.

Mark S. Leeson received the degrees of B.Sc. and B.Eng. with First Class Honors in Electrical and Electronic Engineering from the University of Nottingham, UK, in 1986. He then obtained a Ph.D. in Engineering from the University of Cambridge, UK, in 1990. From 1990 to 1992 he worked as a Network Analyst for National Westminster Bank in London. After holding academic posts in London and Manchester, in 2000 he joined the School of Engineering at Warwick, where he is now a Reader. His major research interests are coding and modulation, nanoscale communications and evolutionary optimization. To date, Leeson has over 230 publications and has supervised fifteen successful research students. He is a Senior Member of the IEEE, a Fellow of Both the Institute of Physics and the UK Higher Education Academy.

Matthew D. Higgins received his M.Eng. in Electronic and Communications Engineering and Ph.D. in Engineering from the School of Engineering at the University of Warwick in 2005 and 2009 respectively. Remaining at the University of Warwick, he then progressed through several Research Fellow positions with leading defense and telecommunications companies before undertaking two years as a Senior Teaching Fellow. From July 2012 until February 2016, he was an Assistant Professor in the School of Engineering. As of March 2016, Higgins holds the position of Associate Professor in the Warwick Manufacturing Group (WMG), University of Warwick. His major research interests include the modelling of optical propagation characteristics in underwater, indoor and atmospheric conditions as well as investigating new areas such as nano-communications. Higgins is a Member of the IEEE.